THE ASTROPHYSICAL JOURNAL, 460:460–469, 1996 March 20

REFRACTIVE AND DIFFRACTIVE SCINTILLATION OF THE PULSAR PSR B0329+54

DANIEL R. STINEBRING AND MICHAEL D. FAISON[1]
Department of Physics, Oberlin College, Oberlin, OH 44074

AND

MARK M. MCKINNON
National Radio Astronomy Observatory,[2] Green Bank, WV 24944
Received 1994 November 28; accepted 1995 September 21

ABSTRACT

Refractive and diffractive scintillation are thought to be two related consequences of scattering in the interstellar medium. The predicted modulation of diffractive scintillation parameters by refractive effects has not been thoroughly tested, however. We report 24 days of scintillation observations of the radio pulsar PSR B0329+54 from 1993 September to 1994 June with a 26 m telescope operating at 610 MHz. Dynamic spectra were obtained on each day, from which the characteristic bandwidth and timescale of the diffractive scintillation pattern were determined. A relative flux value for the pulsar was also obtained on each day. The cross-correlation coefficient for each unique pair of the observables—flux, δF, bandwidth, $\delta\nu$, and timescale, δt—was formed from these data. The observed values of these coefficients and their 67% confidence-intervals are: $C_{\delta F\,\delta\nu} = -0.4 \pm 0.2$, $C_{\delta F\,\delta t} = -0.7 \pm 0.1$, and $C_{\delta\nu\,\delta t} = 0.5 \pm 0.2$. Theoretical expectations are that $C_{\delta F\,\delta\nu} = -0.8$, $C_{\delta F\,\delta t} = -0.6$, and $C_{\delta\nu\,\delta t} = 0.8$. We conclude that we have detected the expected modulation of diffractive parameters by refractive scintillation. This adds confidence to the interpretation that diffractive and refractive scintillation of compact radio sources are caused by the same underlying scattering process.

Subject headings: ISM: structure — pulsars: individual (PSR B0329+54) — radio continuum: stars

1. INTRODUCTION

If the interstellar medium were homogeneous, radio waves from pulsars would be affected by dispersion from the ionized component of the gas, but would otherwise be uninfluenced by the propagation over kiloparsecs. The angular size of a typical pulsar would be something less than a microarcsecond. Instead, pulsar angular sizes are often inferred or measured to be milliarcseconds in size, providing evidence that substantial scattering of the radio waves is taking place in the interstellar medium.

Scattering in the interstellar medium is a complicated and multifaceted subject, both because little is definitely known about the density inhomogeneities that scatter the radio waves and because this is a theoretically challenging problem. Nevertheless, much observational and theoretical progress has been made on various aspects of the problem, as reviewed by Rickett (1990).

What has become known as *diffractive interstellar scintillation* (DISS), and what was the original pulsar scintillation observed by pulsar discoverers Hewish et al. (1968), includes such well-known effects as the angular broadening of galactic and extragalactic radio sources, the rapid (minutes to hours) variation of the radio flux from pulsars, the scatter-broadening of short time features in the pulsar signal, and the random corrugation in time and frequency imposed on the spectrum of pulsars by interstellar propagation. These diffractive effects are thought to arise from inhomogeneities in the free electron density of the interstellar medium with a typical scale size of 10^6–10^8 m. In the early 1980s another class of propagation effects was discovered (Sieber 1982; Rickett, Coles & Bourgois 1984). This has become known as *refractive interstellar scintillation* or RISS and includes the long-term (days to years) variation of pulsar fluxes, as well as more subtle effects due to gradients or curvature in the interstellar density profile on size scales comparable to that of the cross section of the scattered ray bundle. For typical pulsars observed in the frequency range of 0.3–1.0 GHz, the size of these inhomogeneities is roughly 10^{11}–10^{13} m (see Armstrong, Rickett, & Spangler 1995 for more details).

Since its initial identification, RISS has generated much theoretical and observational interest, since it is relevant to a number of outstanding problems in radio astronomy (Rickett 1986). Examples of theoretical treatments that stay close to observational issues are papers by Cordes, Pidwerbetsky, & Lovelace (1986, hereafter CPL) and Romani, Narayan, & Blandford (1986, hereafter RNB). On the observational side, data from a number of groups (Stinebring & Condon 1990; Rickett & Lyne 1990; Kaspi & Stinebring 1992 [hereafter KS]; Gupta, Rickett, & Coles 1993; LaBrecque, Rankin, & Cordes 1994; Gupta, Rickett, & Lyne 1994) have better characterized RISS phenomena and demonstrated that long-term pulsar flux variations are dominated by refractive effects (KS).

Refraction by larger scale structures in the interstellar medium is predicted to influence the more easily observable diffractive effects (CPL, RNB). A number of authors have addressed the effects of refraction on the dynamic spectra of pulsars, most recently Gupta et al. (1994) (see also CPL; Roberts & Ables 1982; Hewish, Wolszczan, & Graham 1985; Smith & Wright 1985; Wolszczan & Cordes 1987). These studies concentrate, by and large, on the relatively frequent appearance of *fringing* or *periodic modulation* patterns in dynamic spectra, an observation that is not consistent with a Kolmogorov spectrum of density inhomogeneities, as emphasized by Gupta et al. (1994).

[1] Department of Astronomy, University of Wisconsin, Madison, WI 53706.

[2] The National Radio Astronomy Observatory is a facility of the National Science Foundation operated under cooperative agreement by Associated Universities, Inc.

We present here an observational study of the correlation between pulsar flux—a measurement of refractive effects—and two diffractive observables: decorrelation bandwidth, v_d, and decorrelation timescale t_d. We know of only one previous observational study that has addressed this issue directly, that of Cognard et al. 1995 (also see Lestrade, Cognard, & Biraud 1995). They found an anticorrelation between pulsar flux and pulse time of arrival in high-precision timing data of the millisecond pulsar PSR B1937+21. Not only does this demonstrate a connection between refractive and diffractive scintillation but they interpret the negative correlation coefficient between these observables as indicating that this line of sight is dominated by small-scale irregularities, consistent with a Kolmogorov density spectrum (Blandford & Narayan 1985). In this paper we present another such study, using an approach that should be applicable to a much broader range of pulsars.

Let us first consider one such effect qualitatively. Refractive effects can be thought of as a squeezing, stretching, or lateral displacement of the ray bundle that reaches the telescope. In some cases the ray bundle can split into multiple pieces (Narayan & Goodman 1989a, b). Since the diffractive observables depend on the distribution of path length differences in the ray bundle, the refractive distortions of the ray bundle will naturally give rise to modulation of diffractive parameters. For example, a widening of the ray bundle due to the interposition of a focusing inhomogeneity along the line of sight will give rise to an increase in flux density due to the increased number of rays reaching the telescope. This widening of the ray bundle also spreads out the range of path lengths reaching the telescope. We would thus expect that the impulse response of the interstellar medium or, using different terminology, the scatter-broadening time of pulse features in the time domain should be increased by this focusing event. Equivalently, this increase in the relative path lengths reaching the observer should give rise to a decreased bandwidth of scintillation features in the pulse spectrum, since the scatter broadening time, τ_s, and the decorrelation bandwidth are related by an uncertainty relation, $2\pi v_d \tau_s \approx 1$ (see, e.g., Rickett 1990). Thus we would expect to see a *modulation* of the diffractive parameters by refractive effects. In the case just considered, we expect an increase in pulsar flux to be accompanied by a decrease in decorrelation bandwidth; the decorrelation bandwidth should become wider if the pulsar flux decreases. For the pulsar and observing frequency that we are considering here, it is much easier to observe variations in the "decorrelation bandwidth," v_d, than it is to observe the increase of the impulse response directly.

The anticorrelation between pulsar flux and decorrelation bandwidth is a central prediction of refractive scintillation theory and does not depend sensitively on the spectrum of inhomogeneities that gives rise to the scattering, as is clear from the explicit expressions for this and other correlation coefficients presented by RNB and discussed further below. There is a similar prediction of an anticorrelation between pulsar flux and the characteristic time duration of scintillation maxima in a dynamic spectrum, the "decorrelation timescale", t_d.

In § 2 of this paper we elaborate on the expected relation between refractive and diffractive scintillation, drawing on results from the literature. The observing setup and a summary of the observations are presented in §3. We present the results of 24 days of observations in § 4 and discuss the strength of the correlation between pulsar flux and diffractive scintillation parameters. We discuss these results and present our conclusions in § 5.

2. THEORY

We are concerned here with the cross-correlation[3] between various observable quantities. In particular, we are interested in the cross-correlation of radio flux, F, decorrelation bandwidth, v_d, and decorrelation timescale, t_d. Although many theoretical treatments of radio wave scattering exist, most of these focus on how observable quantities scale with observing frequency, location of the scattering screen, thickness of the scattering screen, and strength of scattering (e.g., CPL). These authors calculate the depth of refractive flux modulation under the assumption of a power-law inhomogeneity spectrum

$$Q(q) = C_N^2 q^{-\beta}, \tag{1}$$

where q is the spatial wavenumber of the fluctuation, C_N^2 characterizes the strength of the scattering, and the power-law index β indicates the steepness of the inhomogeneity spectrum. The value of β determines whether the scattering is better thought of as a turbulence spectrum ($\beta < 4$, referred to as type A by CPL) or is best characterized as a stochastic superposition of discrete scattering structures ($\beta > 4$, referred to as type B by CPL)[4]

We know of only one series of papers in which the cross-correlation between observable quantities is explicitly calculated (Blandford & Narayan 1985; RNB). They employ a model that idealizes the short-wavelength (diffractive) and long-wavelength (refractive) density fluctuations as distinct scales in the medium rather than two ranges of scales in an extended spectrum of inhomogeneities. Furthermore, their main results are obtained for a model that places all the scattering in a thin screen with rays striking the screen from an infinitely distant pulsar. Although these seem like drastic simplifications of a much more complicated scattering situation, there is observational evidence (e.g., KS; Gupta, et al. 1993) that this analysis properly predicts the depth of refractive flux modulation and the timescale on which those fluctuations occur.

With these approximations, the RNB *two-scale* formalism can be employed to calculate auto- and cross-correlation functions analytically. Leaving out the details provided by Blandford & Narayan (1985) and RNB, the procedure is as follows. A normalized fluctuation of an observable is found by integrating an *intensity-weighted* multiple of the phase of the electromagnetic wave over the image on the phase-changing screen. The image is assumed to have a Gaussian intensity profile, $I = I_0 \exp(-r^2/\sigma^2)$, where $\sigma \sim \theta L/2$ is the image size on the screen and θ is the observed angular diameter of the source. The weighting function employed is dependent on the observable in question. This gives rise to two classes of observable fluctua-

[3] We, in fact, consider the cross-covariance, i.e., the cross-correlation between deviations from the mean, but we will continue to use the more familiar cross-correlation terminology when no confusion is likely to result.

[4] See Armstrong et al. (1995) for a discussion of observational support for a power-law form of the density inhomogeneity spectrum over many orders of magnitude of wavenumber.

tions: (I) *curvature-induced fluctuations* which depend on the average second derivative of the electromagnetic phase integrated over the image and (II) *gradient-induced fluctuations* which depend on the first-derivative of the phase. The quantities of interest here, F, v_d, and t_d are all members of the curvature-induced class. This is important because it is only between members of the same class that cross-correlation of the fluctuations is expected to be observable. Following the RNB formalism, we have calculated the cross-correlation functions for the three observables of interest here (see the Appendix).

Although, in principle, it would be good to compare an observed cross-correlation function with the theoretical function, in practice our observations are too coarsely and unevenly spaced to make a meaningful comparison with the functional form. As presented below, however, we are able to compare the zero-lag values of the cross-correlation functions (the cross-correlation *coefficients*) with observations. The auto- and cross-correlation coefficients, tabulated by RNB are reproduced here in Table 1. These are identical to the zero-lag values of our equations (A12)–(A14). Notice that, irrespective of the value of β, the cross-correlation coefficient between flux and decorrelation bandwidth is large and negative (≈ -0.8), that between flux and decorrelation timescale is large and negative (≈ -0.6), and that between bandwidth and timescale is large and positive (≈ 0.8).

RNB treat the case of multiple scattering screens as well as the continuum limit of a continuous scattering medium. They find that the single-screen case underestimates the refractive flux variations by roughly a factor of 2 (dependent on β). They also note that the cross-correlation at zero lag of the angular size of the source and the flux is 0.75 times the single-screen value. Although we have not investigated the continuous medium case for the cross-correlations under study here, it seems likely that the continuous medium values will not vary greatly from the single-screen predictions.

As noted in the Introduction, CPL have also presented an extensive analysis of the pulsar scattering problem. Using a one-dimensional scattering geometry, CPL present explicit expressions for the observables of interest here (F, v_d, and t_d) in terms of the first and second derivatives of the electromagnetic phase emerging from the scattering screen. Their assumptions are similar to those presented by Blandford & Narayan (1985) and RNB, although the emphasis of their analysis is different. CPL do not directly address the issue of cross-correlation of observables, although one could use their expressions for the observable parameters in a suitable simulation to determine ensemble-averaged cross-correlation coefficients. They also address the two-dimensional and three-dimensional cases, concluding that cross-correlations between observable parameters will be qualitatively similar to the one-dimensional case, but will be reduced quantitatively by the additional degrees of freedom.

Similarly, Gupta, Rickett, & Lyne (1994) present thoretical predictions for the observables of interest here using a two-dimensional screen and a Taylor expansion of the electromagnetic phase as in RNB and CPL. They also do not directly address the coefficient issue, however. Again it would be possible to use their results and a phase-screen simulation to obtain cross-correlation coefficients.

In summary, the most complete theoretical treatment of cross-correlations between observables, that of RNB, yields a high degree of *anti*correlation between flux and either diffractive bandwidth or diffractive timescale and a high positive correlation between diffractive bandwidth and timescale. Note that this is a two-dimensional, analytical treatment of the situation with indications that a three-dimensional extension of the theory yields qualitatively similar results. None of the other theoretical treatments of which we are aware contradicts the basic conclusions of RNB with regard to the strength of these cross-correlation coefficients.

TABLE 1

CROSS-COVARIANCE AND AUTOCOVARIANCE COEFFICIENTS[a]

Coefficient	$\beta = 3.67$	$\beta = 4.00$	$\beta = 4.30$
$C_{\delta F\, \delta v}(0)$	−0.76	−0.80	−0.84
$C_{\delta F\, \delta t}(0)$	−0.50	−0.58	−0.64
$C_{\delta v\, \delta t}(0)$	0.77	0.79	0.79
$R_{\delta F\, \delta F}(0)/K$	1.04	1.00	1.00
$R_{\delta v\, \delta v}(0)/K$	0.78	0.87	1.01
$R_{\delta t\, \delta t}(0)/K$	0.18	0.19	0.20

[a] As calculated by Romani, Narayan, & Blandford (1986). The value of β characterizes the steepness of the density inhomogeneity spectrum, with $\beta = 3.67$ being the Kolmogorov value and $\beta = 4.30$ representative of a steep spectrum. See RNB for details.

3. OBSERVATIONS

The observations were made with a 26 m telescope at the National Radio Astronomy Observatory (NRAO) in Green Bank, West Virginia. The US Naval Observatory employs the telescope (known locally as 85-3) as an element of a very long baseline interferometer for about 80 hr a week. During the remainder of the time the telescope is used in an automated program to time pulsars and monitor pulsar flux densities on a daily basis with our automated pulsar data acquisition system ("the pulsar Mark III system"; Stinebring et al. 1992; KS). The detector used for these observations was the NRAO spectral processor, a digital fast Fourier transform spectrometer. The spectral processor is a dedicated backend to the NRAO 42 m telescope, which is located about a mile away from the 26 m. The spectral processor is linked to the 26 m telescope by a fiber optic cable. Thus we were able to conduct our observations only on days when both the 26 m telescope was used in the pulsar monitoring program and the spectral processor was available at the 42 m telescope.

Our observations were made at a sky frequency of 610 MHz with 20 MHz of bandwidth and dual linearly polarized feeds. The spectral processor was configured to produce a 256-channel spectrum in each polarization, giving a frequency resolution of 78 kHz. Spectra were binned into 128 time bins across the entire pulsar period, resulting in a time resolution of 5.6 ms, which is approximately the full width at half-maximum of the pulse. Thus, we have little information about the variation of the spectrum across the pulse. Spectra in the two polarizations were collected once every 60 s and written to magnetic tape for off-line analysis. The duration of a single observation was about 90 minutes.

In addition to the spectral processor data-taking, we also obtained data with the pulsar Mark III system referred to

TABLE 2

OBSERVATIONAL SUMMARY

Date	MJD	Duration (minutes)	Flux (Jy)	Δv_d (kHz)	Δt_d (s)
1993 Sep 18	49248	74	1.14 ± 0.03	380 ± 50	340 ± 30
1993 Nov 19.....	49310	106	1.27 ± 0.03	470 ± 70	300 ± 30
1993 Nov 20.....	49311	107	1.64 ± 0.05	400 ± 60	320 ± 30
1993 Nov 21.....	49312	107	1.11 ± 0.03	340 ± 40	310 ± 30
1994 Feb 18	49401	63	0.69 ± 0.04	470 ± 90	470 ± 60
1994 Feb 19	49402	108	0.94 ± 0.05	400 ± 60	330 ± 30
1994 Feb 20	49403	108	0.97 ± 0.03	480 ± 90	420 ± 50
1994 Feb 21	49404	108	0.85 ± 0.05	470 ± 90	460 ± 60
1994 Feb 23	49406	106	0.91 ± 0.04	380 ± 50	330 ± 30
1994 Feb 24	49407	109	1.04 ± 0.04	520 ± 110	490 ± 70
1994 Feb 25	49408	95	0.66 ± 0.03	300 ± 40	370 ± 30
1994 Feb 27	49410	108	0.85 ± 0.06	370 ± 50	380 ± 40
1994 Feb 28	49411	108	0.74 ± 0.03	300 ± 40	370 ± 30
1994 Mar 13.....	49424	63	0.90 ± 0.05	430 ± 70	370 ± 40
1994 Apr 15	49457	86	0.96 ± 0.03	380 ± 60	380 ± 40
1994 Apr 17	49459	87	0.83 ± 0.02	370 ± 50	360 ± 40
1994 Jun 4.....	49507	46	1.25 ± 0.04	240 ± 30	320 ± 20
1994 Jun 5.....	49508	79	1.15 ± 0.03	230 ± 30	400 ± 30
1994 Jun 6.....	49509	90	1.14 ± 0.03	250 ± 30	350 ± 30
1994 Jun 9.....	49512	81	1.45 ± 0.03	280 ± 30	330 ± 30
1994 Jun 10	49513	41	1.33 ± 0.04	210 ± 20	260 ± 20
1994 Jun 11	49514	49	1.25 ± 0.04	250 ± 30	280 ± 20
1994 Jun 12	49515	85	1.27 ± 0.03	210 ± 20	300 ± 20
1994 Jun 23	49526	91	1.48 ± 0.04	240 ± 20	260 ± 20
Mean.....	...	...	1.08	349	354

above. In this case we obtained total intensity average profiles of the pulsar in 16 × 1 MHz channels with 256 time bins across the pulse period. In addition a noise diode calibration signal was turned on in synchronism with the data-taking at the beginning of the run in order to calibrate the gain of each receiver channel. An independent analysis of long-term pulsar flux variations over 800 days using this relative flux calibration has shown no variation in the strength of the calibration signal above the 5% variation of the most stable pulsar in our flux-monitoring program and no common-mode signal between pulsars (KS; Stinebring et al. 1995). We, therefore, believe that the flux values determined from the Mark III data are accurate on a relative flux scale to 5% of the mean flux value. The conversion from flux in terms of noise calibration height to flux in janskys has been accomplished by assuming a noise calibration signal of 5.0 K and a telescope gain of 0.1 K Jy^{-1}. The resulting absolute flux values are accurate to no better than 20%, but this is not relevant to the analysis that follows since we are interested only in *relative* flux variations for the purposes of this paper.

In the following analysis we used the spectral processor data to obtain frequency and timescale information about the scintillation structure and the pulsar Mark III system to obtain flux values. The two data-taking systems were run simultaneously and were fed the same intermediate-frequency signal. Using these two systems we obtained a total of 24 usable observations of PSR B0329+54 between 1993 September 18 and 1994 June 24, as summarized in Table 2.[5]

[5] Following Taylor, Manchester, & Lyne (1993), the designation B0329+54 refers to the 1950.0 coordinate epoch; the J2000 coordinate designation for this pulsar is J0332+5434.

4. ANALYSIS AND RESULTS

The two polarization channels from a single integration were added together to improve the signal-to-noise ratio of the data. The resulting spectra from the consecutive integrations were then stacked to produce a dynamic spectrum, a three-dimensional data matrix with axes corresponding to frequency, time, and intensity. We present the dynamic spectra as gray-scale plots with the horizontal axis corresponding to frequency, the vertical axis corresponding to time, and the darkness of the gray scale corresponding to intensity (Fig. 1). The dynamic spectra show modulation of the pulsar intensity in both frequency and time. Areas of maximum intensity are known as "scintles" and have a characteristic size in frequency and time referred to as the decorrelation bandwidth and decorrelation timescale, respectively. The scintles may also show a tilting or drifting in frequency, a phenomenon that was not evident in our data and that will not be pursued further here.[6] To measure the characteristic bandwidth and timescale of the scintles, we calculated the two-dimensional autocorrelation function of each dynamic spectrum (Fig. 2). We then fitted a two-dimensional Gaussian function of the form

$$\rho(\nu, t) = A + B \exp\left[-(c_1\nu^2 + c_2\nu t + c_3 t^2)\right], \quad (2)$$

to the autocorrelation function (see Gupta et al. 1994 for justification)., where ν and t are the lags in frequency and time, respectively. The fit was done by iterative least squares using a grid search algorithm. Following the convention of Cordes, Weisberg, & Boriakoff (1985), we define the decor-

[6] An absence of tilting or periodicity of scintles in the dynamic spectrum means that the dominant refractive effect is a broadening or narrowing of the ray bundle rather than an elongation or bifurcation as can occur in more extreme cases of refraction.

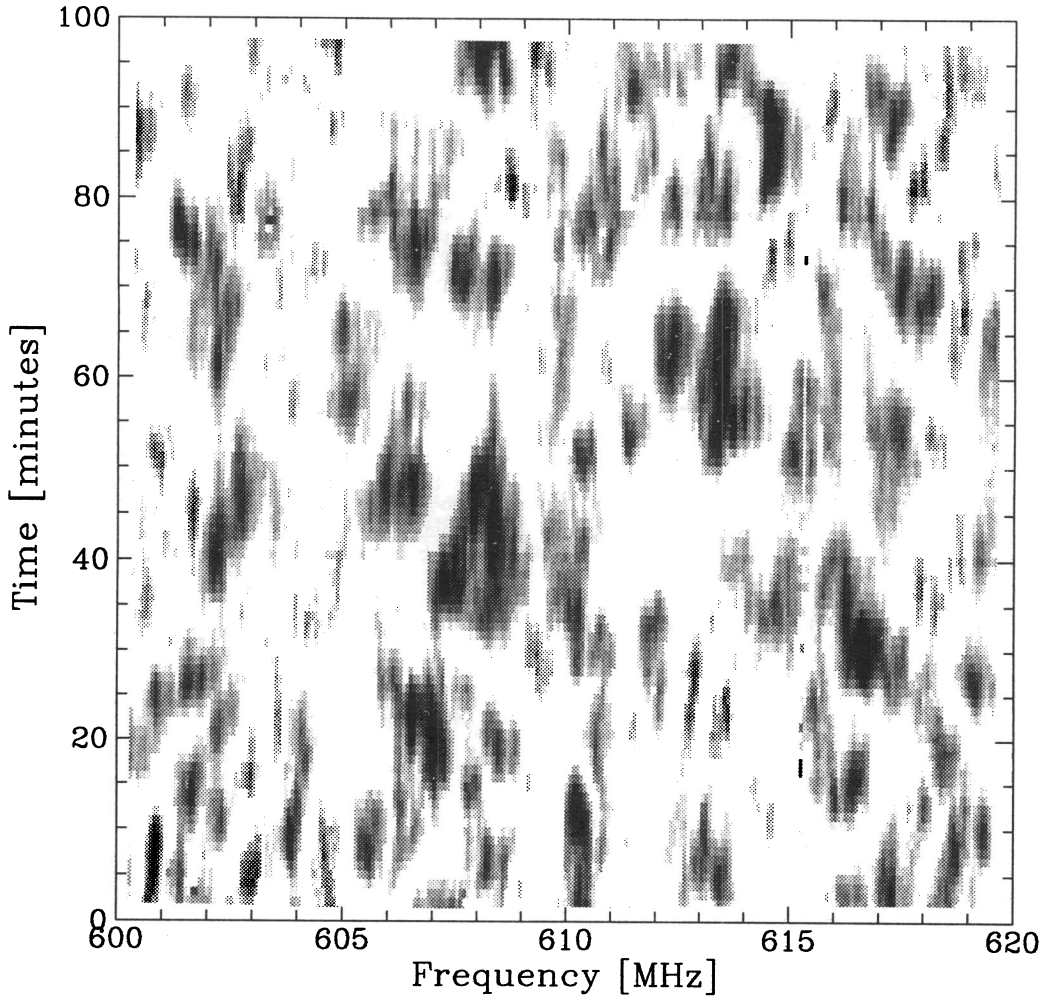

FIG. 1.—Dynamic spectrum of PSR 0329+54 taken 1993 November 22. The horizontal axis corresponds to frequency, and the vertical axis corresponds to time. The darkness of the gray scale indicates the intensity and is scaled linearly such that black indicates the top 5% of the data and white indicates the bottom 25% of the data. The total bandwidth observed is 20 MHz in 256 frequency channels, centred at 610 MHz. The resolution of each frequency channel is 78.1 kHz. Narrow-band interference can be seen in two of the frequency channels. The total observing time was 100 minutes. Each row in the dynamic spectrum is a spectrum integrated over 1 minute of observing time. The intensity maxima have a characteristic bandwidth and fade time that is determined by fitting a two-dimensional Gaussian function to the autocorrelation function of the dynamic spectrum.

relation bandwidth, v_d, to be the half-width at half-maximum of the Gaussian in frequency, and we define the decorrelation timescale, t_d, to be the half-width at $1/e$ of the maximum of the Gaussian in time. In terms of the fit parameters,

$$v_d = \sqrt{\frac{\ln 2}{c_1}} \tag{3}$$

$$t_d = \sqrt{\frac{1}{c_3}} . \tag{4}$$

The cross term, c_2, describes the tilt of the ellipse, which was close to zero for all the spectra we analyzed.

No absolute flux calibration was performed on the dynamic spectra. The flux density of the pulsar on the days of spectral processor observations was taken from the pulsar flux monitoring project at the 26 m telescope. The pulsar is observed over a wide enough bandwidth and for a long enough integration time (typically 90 minutes) to average the diffractive fluctuations down below the 10% level. The flux error bars are determined from the standard deviation of the multiple flux measurements we made each day with the pulsar Mark III system (typically 6 scans × 16 channels), which are averaged to form the daily flux estimate. We can consider only correlations between diffractive parameters and the flux density on days for which we have both diffractive parameters from the observations with the spectral processor and the flux density from the monitoring project.

Figure 3 shows the time series for the flux, indicating the uneven sampling of the data over 10 months of observations. In Figures 4–6 we present a series of the flux, decorrelation bandwidth, and decorrelation timescale in sequential order of observation to aid in a comparison of the fluctuations in these quantities. Following Cordes et al. (1985) and Roberts & Ables (1982), the errors in the diffractive parameters are determined by estimating the fractional error in the diffractive parameters as $N^{-1/2}$, where N is a rough estimate of the number of scintles in the dynamic spectrum. We calculate N from the decorrelation bandwidth, v_d, and the decorrelation timescale, t_d, as

$$N = \frac{(\text{total observing time} \times \text{total observed bandwidth})}{(v_d \times t_d)} . \tag{5}$$

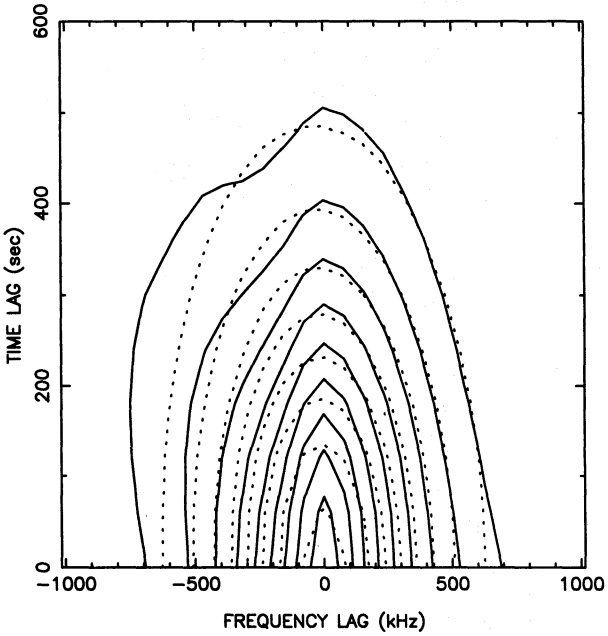

FIG. 2.—Contour plot of the autocorrelation function for the dynamic spectrum in Fig. 1. The solid contours indicate the actual autocorrelation function values, and the dotted contours indicate the two-dimensional Gaussian fit which is used to determine the decorrelation bandwidth and decorrelation timescale. The interval between contours is a tenth of the maximum data value.

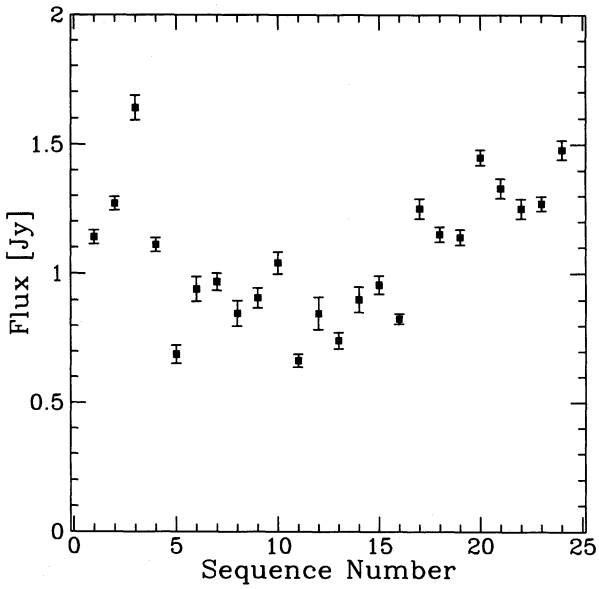

FIG. 4.—Sequential series of the pulsar flux with 1 σ uncertainties, in order of observing sequence. The error estimates are discussed in the text. Observing sequence number has been used as the abscissa rather than the time of observation in order to clearly show each data point. As shown in Fig. 3, the data sampling was far from uniform, occurring in several sessions over an 8 month period.

This fractional error is multiplied by the decorrelation bandwidth or the decorrelation timescale to give the absolute error in those parameters.

In Figures 7–9 we present scatter plots for the three independent pairs of the observables: flux, decorrelation bandwidth, and decorrelation timescale. The dotted lines indicate the unweighted mean of each parameter over the 24 days of observation.

Two types of correlation coefficients were calculated for each of the three independent pairs of observables. The linear correlation coefficient, r, (sometimes referred to as "the Pearson r") of two arrays x and y is given by

$$r = \frac{\sum_i (x_i - \bar{x})(y_i - \bar{y})}{\sqrt{\sum_i (x_i - \bar{x})^2}\sqrt{\sum_i (y_i - \bar{y})^2}} . \quad (6)$$

The Spearman rank-order correlation coefficient, R_s, is a nonparametric correlation coefficient that is calculated by replacing the value of the data point by its rank among the rest of the data. In our case of 24 data points, the data value

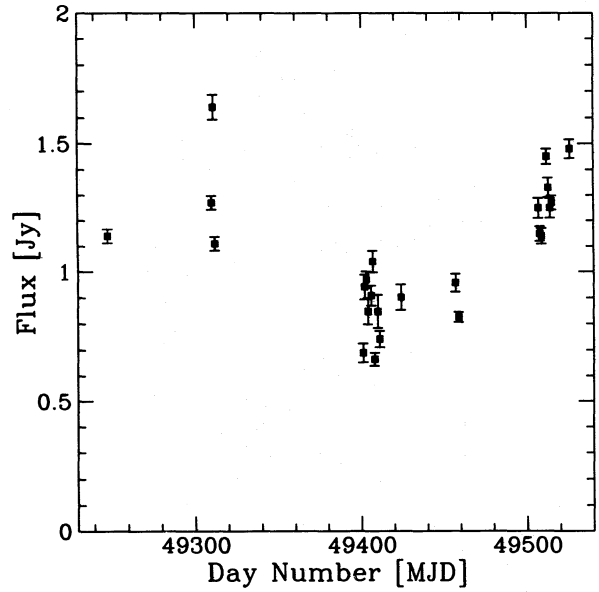

FIG. 3.—Time series of the pulsar flux for the days with corresponding diffractive parameter measurements. Gaps in the time series represent days for which diffractive parameter data were not taken. The observation days on the time axis are given in terms of modified Julian Day number.

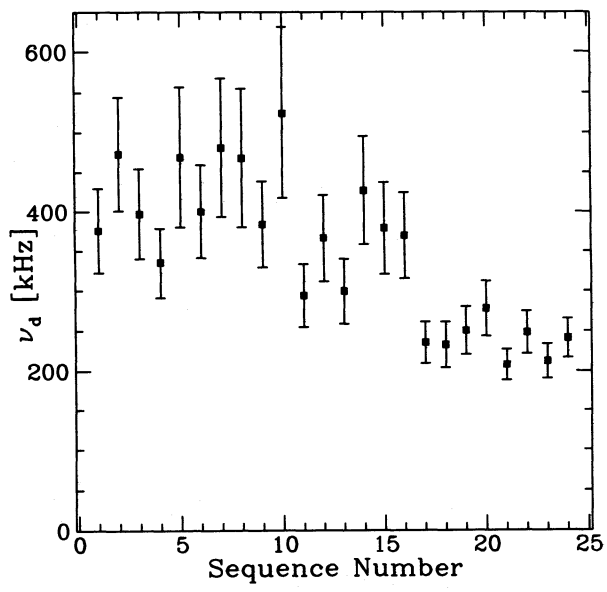

FIG. 5.—Sequential series of the decorrelation bandwidth, ν_d, with 1 σ uncertainties. By convention (Cordes et al. 1985), the decorrelation bandwidth is the half-width at half-maximum along the frequency axis of the autocorrelation function.

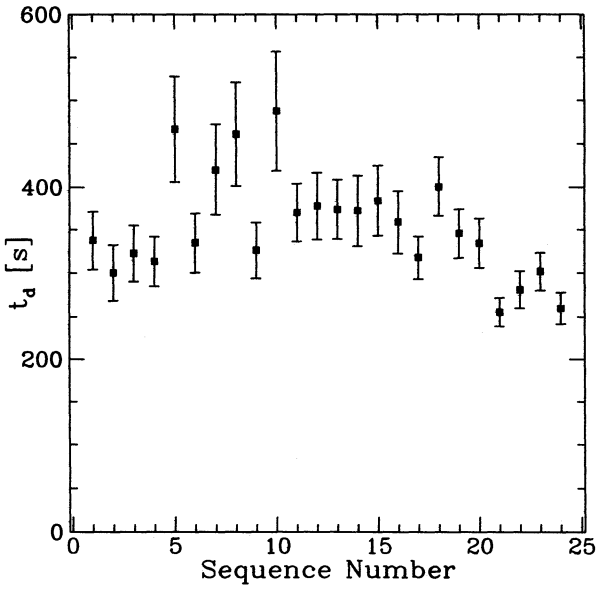

FIG. 6.—Sequential series of the decorrelation timescale, t_d, with 1 σ uncertainties. By convention, the decorrelation timescale is the half-width at $1/e$ along the time axis of the autocorrelation function.

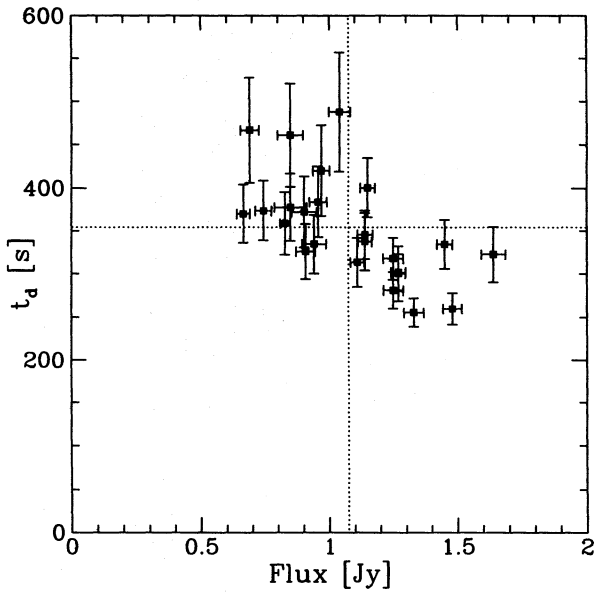

FIG. 8.—Scatter plot of the decorrelation timescale, t_d, vs. the flux. The dotted lines indicate the mean of each parameter. The theoretical prediction for the cross-correlation coefficient of these two observables is $C_{\delta F\, \delta t} = -0.6$. We found a Spearman rank-order correlation coefficient of $C_{\delta F\, \delta t} = -0.7 \pm 0.1$, for these two quantities.

is replaced by an integer from 1 to 24, and a Pearson r correlation coefficient is calculated from these ranks. The coefficient R_s is more robust statistically than the Pearson r because it is less sensitive to outlying points.

In Table 3 we present the Pearson r linear correlation coefficient for decorrelation bandwidth versus flux, decorrelation timescale versus flux, and decorrelation timescale versus decorrelation bandwidth. In Table 4 we present the corresponding Spearman rank-order correlation coefficients. The confidence intervals are determined by creating a *bootstrap* distribution from the 24 points (Efron 1979; Diaconis & Efron 1983). The bootstrap method we used is referred to by Efron as "method 2" and is a Monte Carlo procedure. From the 24 data points, a new sample of 24 values is chosen at random with replacement, so that some of the points can appear more than once in the sample. A new correlation coefficient is calculated from this bootstrap sample; in our case this procedure is repeated 200,000 times. The confidence intervals are determined by integrating the distributions from the wings inward to 33% and 5% of the total area under the distribution curve to give the 67% and the 95% confidence intervals, respectively.

As pointed out by S. Spangler, this procedure still underestimates the uncertainty in our determination of the correlation coefficients since we were not able to sample many independent cycles of any of the observables under study.

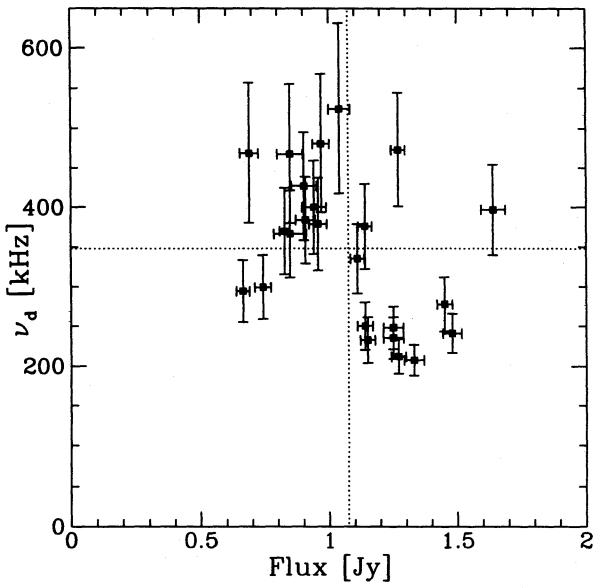

FIG. 7.—Scatter plot of the decorrelation bandwidth, ν_d, vs. the flux. The dotted lines indicate the mean of each parameter. The theoretical prediction for the cross-correlation coefficient of these two observables is $C_{\delta F\, \delta \nu} = -0.8$. We found a Spearman rank-order correlation coefficient of $C_{\delta F\, \delta \nu} = -0.4 \pm 0.2$, for these two quantities.

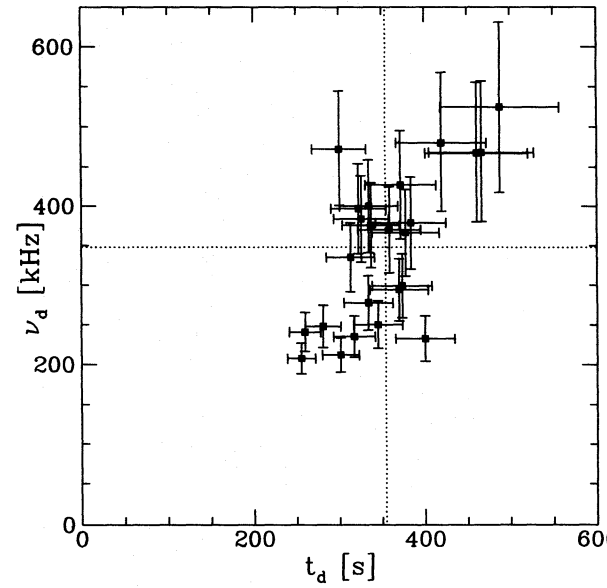

FIG. 9.—Scatter plot of the decorrelation bandwidth, ν_d, vs. the decorrelation timescale, t_d. The dotted lines indicate the mean of each parameter. The theoretical prediction for the cross-correlation coefficient of these two observables is $C_{\delta \nu\, \delta t} = 0.8$. We found a Spearman rank-order correlation coefficient of $C_{\delta \nu\, \delta t} = 0.5 \pm 0.2$ for these two quantities.

TABLE 3

PEARSON r LINEAR CORRELATION COEFFICIENTS WITH CONFIDENCE INTERVALS DETERMINED FROM THE BOOTSTRAP DISTRIBUTIONS

	Pearson r	67% Confidence Interval	95% Confidence Interval
v_d vs. Flux.....	−0.40	−0.57 to −0.26	−0.72 to −0.09
t_d vs. Flux.....	−0.62	−0.71 to −0.55	−0.80 to −0.43
v_d vs. t_d	0.65	0.50 to 0.76	0.27 to 0.84

TABLE 4

SPEARMAN RANK-ORDER COEFFICIENT, R_s, WITH CONFIDENCE INTERVALS DETERMINED FROM THE BOOTSTRAP DISTRIBUTIONS

	Spearman R_s	67% Confidence Interval	95% Confidence Interval
v_d vs. Flux.....	−0.41	−0.62 to −0.28	−0.76 to −0.05
t_d vs. Flux.....	−0.68	−0.79 to −0.62	−0.89 to −0.45
v_d vs. t_d	0.54	0.31 to 0.67	0.05 to 0.79

However, we have sampled a sufficient number of independent cycles to be sure of the basic character of the results presented above. An analysis of 5 yr of nearly daily flux observations of PSR B0329+54 (Stinebring et al. 1995) shows that the refractive timescale for this pulsar (half saturation value of the structure function) is 22 days. As discussed more thoroughly in that work, this compares well with the theoretical predictions for the refractive timescale, which range from 7 days to 33 days depending on theoretical assumptions. Reference to Table 2 and Figure 3 indicate that our data are distributed roughly in five independent clusters separated from each other by more than this refractive timescale. Thus, although we do not sample in many independent fluctuations of the random processes as would be desirable, we do have enough independent samples to be confident of our basic conclusions.

5. DISCUSSION AND CONCLUSIONS

As discussed in § 2, the theoretical consensus is that flux should be strongly anticorrelated with both decorrelation bandwidth and decorrelation timescale, regardless of the steepness of the density inhomogeneity spectrum. Furthermore, decorrelation bandwidth and timescale should be strongly positively correlated. As noted in that section, there are a number of approximations and assumptions that go into those predictions which are not likely to be borne out fully in actuality. It is not likely, for example, that the separation of the electromagnetic phase into two distinct regimes—diffractive and refractive—will be as sharp as is assumed here. The effects of three-dimensional propagation through the interstellar medium have not been modeled in detail, although it has been discussed (CPL; RNB; Gupta et al. 1994). The impact of three-dimensional propagation on the cross-correlation coefficients may be to reduce the strength of correlation. Presumably, at least two-dimensional scattering screens are the norm in the interstellar medium, although observations of enhanced scattering events provide evidence for at least occasional filamentary structures in the scattering material (Fiedler et al. 1987).

In the prediction of cross-correlation coefficients, ensemble averages and time averages have been treated as equivalent. This is clearly not the case, however, unless observations covering many refractive timescales are included in the time average. It is also worth noting that all well-monitored pulsars show significant refractive fluctuations (modulation depth of 20%–40%) on the predicted refractive timescale, whereas instances of phase-gradient induced tilts in dynamic spectra are not as common. Third derivatives of the phase front and high order derivatives have been omitted from modeled effects, and yet the second derivative, curvature-related terms appear to dominate over first derivative, gradient-related effects except in a few nearby pulsars. It seems likely that the mentioned effects will complicate a comparison between ensemble averages and the observational averages we have available.

Furthermore, the noise sources—identified and not identified—in our determination of the observable parameters will serve to decrease the observed cross-correlation coefficients. An inspection of the scatter plots in Figures 7–8 indicates that the noise in the estimation of the parameters may have significantly decreased the absolute value of the cross-correlation coefficient. Of course, unrecognized systematic effects in our observing and analysis procedure could either increase or decrease the degree of cross-correlation.

Turning to the results presented in § 4, we see a statistically signficant cross-correlation between all three pairings of observables. Furthermore, the sign of the cross-correlation coefficient is, in each case, consistent with that expected by theory: flux anti-correlates with both decorrelation bandwidth and timescale, and bandwidth and timescale are positively correlated with each other. The most precise theoretical predictions, summarized in Table 1, indicate values of $C_{\delta F\,\delta v} = -0.8$, $C_{\delta F\,\delta t} = -0.6$, and $C_{\delta v\,\delta t} = 0.8$, whereas we have found $C_{\delta F\,\delta v} = -0.4 \pm 0.2$, $C_{\delta F\,\delta t} = -0.7 \pm 0.1$, and $C_{\delta v\,\delta t} = 0.5 \pm 0.2$. We consider this to be confirmation of the prediction that refractive scintillation modulates diffractive scintillation.

Although these results confirm this important link between refractive and diffractive effects, more work is clearly needed. We plan to continue our observations of PSR B0329+54 to see how these results hold up as more data are acquired. It would be good to expand these observations to more pulsars. We could then see if the result is replicated along different lines of sight. We hope that these observations will provide impetus for further theoretical work in this area, including the consideration of correlations when the refractive flux variations are not small.

We thank the US Naval Observatory for allowing us to use the 26 m telescope when it was not in use for their observations. The NRAO Green Bank staff, particularly R. Fisher, M. Clark, S. White, and W. Shank, were of great assistance in this project. We benefited greatly from conversations with and the assistance of D. Nice. Oberlin students J. Hovis and R. Swartz made valuable contributions to the data analysis. R. Foster and J. Cordes provided important software assistance. We thank S. Spangler for several important suggestions during final preparation of this paper. This work was supported by National Science Foundation grant AST 93-17605.

APPENDIX A

CROSS-CORRELATION FUNCTIONS

Romani et al. (1986) present a simple scattering model that can be used to calculate autocorrelation and cross-correlation functions for a wide range of observable parameters, among them flux, F, decorrelation bandwidth, v_d, and decorrelation timescale, t_d. Although they present normalized cross-correlation coefficients for these quantities in Table 2 of their paper, they do not present analytic expressions for the cross-correlation functions or the zero-lag value, the cross-correlation coefficient. Using the formalism they have developed, we present these functions for the three observables considered in this paper. For convenience we cite the equation numbers of their paper, where relevant. They introduce the function (RNB eq. [2.11]):

$$h_n^\alpha(s) \equiv \int_0^\infty (q\sigma)^{(2n+3-\beta)} \exp\left(\frac{-q^2\sigma^2}{2}\right) J_\alpha(sq)d(q\sigma)$$
$$= \left(\frac{s^2}{2\sigma^2}\right)^{\alpha/2} \frac{2^{(n+1-\beta/2)}}{\Gamma(\alpha+1)} \Gamma\left(n+2+\frac{\alpha-\beta}{2}\right) M\left(n+2+\frac{\alpha-\beta}{2}, \alpha+1, -\frac{s^2}{2\sigma^2}\right), \quad \text{(A1)}$$

where $M(a, b, x)$ is the confluent hypergeometric function (Abramowitz & Stegun 1970).

The following combinations of these functions are useful (RNB eq. [2.12]:

$$g_n^0(s) = h_n^0(s), \quad \text{(A2)}$$
$$g_n^2(s) = \tfrac{1}{2}h_n^0(s) - \tfrac{1}{2}h_n^2(s), \quad \text{(A3)}$$
$$g_n^4(s) = \tfrac{3}{8}h_n^0(s) - \tfrac{1}{2}h_n^2(s) + \tfrac{1}{8}h_n^4(s). \quad \text{(A4)}$$

Using these definitions, Romani et al. (1986) find the autocovariance functions (their eqs. [A13], [A21], and [A22])

$$R_{\delta F\,\delta F}(s) = Kg_1^0(s), \quad \text{(A5)}$$
$$R_{\delta v\,\delta v}(s) = \tfrac{9}{4}K[g_1^0(s) - \tfrac{2}{3}g_2^0(s) + \tfrac{11}{72}g_3^0(s) - \tfrac{1}{72}g_4^0(s) + \tfrac{1}{2304}g_5^0(s)], \quad \text{(A6)}$$
$$R_{\delta t\,\delta t}(s) = K[g_1^4(s) - \tfrac{1}{2}g_2^4(s) + \tfrac{1}{16}g_3^4(s)], \quad \text{(A7)}$$

where the dimensionless constant K (the flux variance) is given in RNB, equations (7.2), (7.4), and (7.7). Note that at zero spatial lag ($s = 0$), we have

$$g_n^0(0) = h_n^0(0), \quad \text{(A8)}$$
$$g_n^2(0) = \tfrac{1}{2}h_n^0(0), \quad \text{(A9)}$$
$$g_n^4(0) = \tfrac{3}{8}h_n^0(0), \quad \text{(A10)}$$

and

$$h_n^0(0) = 2^{n+1-\beta/2}\Gamma(n+2-\beta/2). \quad \text{(A11)}$$

Following the procedure detailed in RNB, we have determined the normalized cross-variance functions for $\delta F, \delta v_d$, and δt_d. These functions are

$$C_{\delta F\,\delta v}(s) = \frac{-3K[g_1^0(s) - (1/3)g_2^0(s) + (1/48)g_3^0(s)]}{2[R_{\delta F\,\delta F}(0)R_{\delta v\,\delta v}(0)]^{1/2}}, \quad \text{(A12)}$$

$$C_{\delta F\,\delta t}(s) = \frac{-K[g_1^2(s) - (1/4)g_2^2(s)]}{[R_{\delta F\,\delta F}(0)R_{\delta t\delta t}(0)]^{1/2}}, \quad \text{(A13)}$$

$$C_{\delta v\,\delta t}(s) = \frac{3K[g_1^2(s) - (7/12)g_2^2(s) + (5/48)g_3^2(s) - (1/192)g_4^2(s)]}{2[R_{\delta v\,\delta v}(0)R_{\delta t\,\delta t}(0)]^{1/2}}. \quad \text{(A14)}$$

REFERENCES

Abramowitz, M., & Stegun, J. A. 1970, Handbook of Mathematical Functions (New York: Dover)
Armstrong, J. W., Rickett, B. J., & Spangler, S. R. 1995, ApJ, 443, 209
Blandford, R. D., & Narayan, R. 1985, MNRAS, 213, 591
Cognard, I., Bourgois, G., Lestrade, J.-F., Biraud, F., Aubry, D., Darchy, B., & Droughin, J.-P. 1995, A&A, 296, 169
Cordes, J. M., Pidwerbetsky, A., & Lovelace, R. V. E. 1986, ApJ, 310, 737 (CPL)
Cordes, J. M., Weisberg, J. M., & Boriakoff, V. 1985, ApJ, 288, 221
Diaconis, P., & Efron, B. 1983, Sci. Am., 248, no. 5, 116
Efron, B. 1979, Ann. Stat., 7, 1
Fiedler, R. L., Dennison, B., Johnston, K. J., & Hewish, A. 1987, Nature, 326, 675
Gupta, Y., Rickett, B. J., & Coles, W. A. 1993, ApJ, 403, 183
Gupta, Y., Rickett, B. J., & Lyne, A. G. 1994, MNRAS, 269, 1035
Hewish, A., Bell, S. J., Pilkington, J. D. H., Scott, P. F., & Collins, R. A. 1968, Nature, 217, 709
Hewish, A., Wolszczan, A., & Graham, D. A. 1985, MNRAS, 213, 167
Kaspi, V. M., & Stinebring, D. R. 1992, ApJ, 392, 530 (KS)
LaBrecque, D. R., Rankin, J. M., & Cordes, J. M. 1994, AJ, 108, 1854
Lestrade, J., Cognard, I., & Biraud, F. 1995, in Proc. ASP Conf. Ser. 72, Millisecond Pulsars: A Decade of Surprise, ed. A. Fruchter, M. Tavani, & D. Backer (San Francisco: ASP), 357
Narayan, R., & Goodman, J. 1989a, MNRAS, 238, 963
———. 1989b, MNRAS, 238, 995
Rickett, B. J. 1986, ApJ, 307, 564

Rickett, B. J. 1990, ARA&A, 28, 561
Rickett, B. J., Coles, W. A, & Bourgois, G. 1984, A&A, 134, 390
Rickett, B. J., & Lyne, A. G. 1990, MNRAS, 244, 68
Roberts, J. A., & Ables, J. G. 1982, MNRAS, 201, 1119
Romani, R. W., Narayan, R., & Blandford, R. 1986, MNRAS, 220, 19 (RNB)
Sieber, W. 1982, A&A, 113, 311
Smith, F. G., & Wright, W. C. 1985, MNRAS, 214, 97
Stinebring, D. R., & Condon, J. J. 1990, ApJ, 352, 207
Stinebring, D. R., Kaspi, V. M., Nice, D. J., Ryba, M. F., Taylor, J. H., Thorsett, S. E., & Hankins, T. H. 1992, Rev. Sci. Instrum., 63, 3551
Stinebring, D. R., Smirnova, T., Hankins, T. H., Hovis, J., Kaspi, V., Kempner, J., Myers, E., & Nice, D. 1995, in preparation
Taylor, J. H., Manchester, R. N., & Lyne, A. G. 1993, ApJS, 88, 529
Wolszczan, A., & Cordes, J. M. 1987, ApJ, 320, L35